JOURNAL OF OPTOELECTRONICS AND ADVANCED MATERIALS Vol. 9, No. 8, August 2007, p. 2468 - 2479

Characterization of pulsed laser deposition plasmas using fast-framing photography and emission spectroscopy

D. MIU*, A. MARCU, C. GRIGORIU, K. YATSUI[a]
National Institute for Laser, Plasma and Radiation Physics, P.O. Box MG-36, Bucharest, Romania
[a]Nagaoka Technical University, Laboratory of Beam Technology, Nagaoka, Niigata 940-21, Japan

Fast-framing photography and optical emission spectroscopy were used to study the expansion of a Pulsed Laser Deposition plasma obtained by irradiating a $YBa_2Cu_3O_{7-x}$ high-temperature superconducting target using an excimer laser. The effects of primary deposition parameters such as laser energy density, gas nature and pressure are presented, and plasma expansion models are used to give phenomenological explanations for Pulsed Laser Deposition plasma behavior. The effect of a polarized electrode placed in the plasma is also assessed. The presence of the electrode can, under certain conditions, preferentially excite oxides over elementary neutrals and ions; this is important in practical deposition conditions, since the presence of oxides is essential for producing high-quality high-temperature superconducting films.

(Received February 28, 2007; accepted June 27, 2007)

Keywords: Pulsed Laser Deposition, Ablation plasma, Thin films, Fast-framing photography, Optical emission spectroscopy

1. Introduction

Pulsed Laser Deposition (PLD) is a method which has proven its capability of producing high-quality films of various materials [1-4]. During the PLD process, which involves deposition of species emitted from the laser-irradiated target onto a nearby substrate, a plasma is formed in the target-substrate region. Many characteristics of such PLD plasmas have a great effect on the quality of the deposited films: the energies of the species, the ion properties or the presence of oxides. It is therefore of interest to study the laser deposition plasma using different experimental methods. In general no one method of plasma analysis allows complete characterization of the plasma, so that complementary methods should be used. Such an analysis of the plasma properties can lead to an optimization of the laser deposition parameters, and therefore of the film properties.

In this paper we present the experimental results obtained for the PLD plasma generated by irradiating a $YBa_2Cu_3O_{7-x}$ (YBCO) high-temperature superconducting target using a KrF excimer laser. The plasma was studied using fast-framing photography and optical emission spectroscopy. The effect of various deposition parameters such as laser energy density, gas nature and pressure, or the effect of a polarized electrode placed in the plasma upon plasma expansion was analyzed. Some phenomenological explanations for the behavior of the PLD plasma are offered, and the extent to which models of the plasma expansion accurately describe the process in our experimental conditions is discussed.

2. Basic aspects of the PLD process

In a typical PLD configuration, the surface of the target is irradiated using laser pulses, and the material thus removed is deposited onto a substrate placed at a distance of the order of several centimeters from the target. The pulse energy density on the target being in the range of hundreds of mJ/cm^2 to J/cm^2 for optimum deposited film properties, the species emitted from the target are ionized, and a plasma is formed in front of the target. At these energy density levels, the plasma generated has a small degree of ionization (typically a few percent), so that its expansion is dictated mostly by the behavior of the neutral species, although it is known that the effects of the ions cannot be neglected [5]. The substrate is heated in order to induce growth of the desired phases and crystalline orientation, to temperatures which depend on the type of material being deposited. The irradiation usually takes place in a gas atmosphere, at pressures ranging from tens to hundreds of mTorr. In the case of High Temperature Superconductors (HTSC), which are oxides, the gas used during deposition is oxygen.

The processes which occur during deposition are complex, and only a general description of the basic phenomena is given here. When the laser beam interacts with the target, the latter is heated, and diffusion of the heat into the solid takes place. This is followed by local melting and evaporation of the target material. Melting is undesirable for good films, since it generates particulates on the film surface; this is minimized for the UV wavelength used in these experiments. Evaporation leads to emission of various species from the target. Expansion of this emitted material can be divided into more regions. In the vicinity of the target there is a high-density region where many collisions between target species occur, leading to increased excitation and ionization and therefore to high luminosity. The behavior of the species in this high density region, which has dimensions of the order of several mm, is independent on ambient gas nature or pressure. In vacuum, beyond the high-density region, the laser ablation plasma undergoes a non-stationary

adiabatic expansion. In this region, the density of the species is still high enough for them to be treated as a continuum, but as they expand, their density further decreases, so that they cease to interact through collisions. Below a critical value of the density the species go into a free expansion, their expansion velocity being constant. In the presence of a gas atmosphere, the behavior of the expanding target species is complicated by interactions with the gas molecules. The processes which occur during the expansion of the PLD plasma in the presence of a gas are either hydrodynamic processes, in which the nature of the gas is not important, or chemical processes, which involve oxidation reactions (in the gas phase or on the surface of the deposited film). Since the oxygen content x in $YBa_2Cu_3O_{7-x}$ is decisive for its superconducting properties, these oxidation reactions, as well as the behavior of oxides in the laser deposition plasma, are very important.

The hydrodynamic models of the laser deposition plasma expansion do not take into account the chemical interactions between the target species and the ambient gas, or the exact nature of the species in the plasma. There are different hydrodynamic models for different domains of the ambient gas pressure [6].

For gas pressures below about 100 mTorr, the effects of the ambient gas are relatively weak, and the propagation of the target species is well described by the "drag" model [7,8]. According to this model, the ablation products are affected by the ambient gas as by a viscous force proportional to their velocity, which leads to a propagation law of the form

$$R = R_f\,[1 - \exp(-\beta t)], \tag{1}$$

where R is the distance from the target, measured along the target normal, R_f is the stopping distance, β is a friction coefficient which is proportional to the ambient gas density, and t is the time.

At gas pressures between about 100 mTorr and 1 Torr, a shock wave is formed in the gas, in front of the ablation products [9,10]. In this situation, the drag model only describes the phenomena well at early expansion moments, before the shock wave is formed, or at late moments, after the shock wave has separated from the ablation species. In the case of PLD of HTSC materials, the moment from which the shock model accurately describes the expansion is about 1÷2 μs from the incidence of the laser pulse onto the target. This moment coincides with that when the mass of the ambient gas which has been "swept up" by the ablation products becomes comparable with the mass of the ablation products. The exact value depends on the pressure of the gas, the total amount of material removed from the target, and the geometry of the expansion, which in turn depends on the dimensions of the laser spot on the target. At this moment, a shock wave is formed in the gas, which slows down the ablation products and leads to their accumulation behind the shock front. For a certain time interval, the ablation products are constrained to move with the shock wave. As they expand, however, the pressure of the ablation products decreases, becoming equal to that of the ambient gas, and the target species separate from the shock wave; from this moment, the shock model no longer describes the propagation of the ablated species. An important observation must be made here. Various analysis methods of the ablation plasma have indicated the presence of a rapid component of the ablation species, which moves ahead of the shock wave without being affected by it for the whole duration of its propagation [11]. A theoretical explanation for the existence of this rapid component was given in [12].

The shock model, which adequately describes the movement of the target species as long as they are constrained to move behind the shock front, offers two different propagation laws, depending on the geometry of the expansion [13]. In the case of a spherical expansion, the propagation law is

$$R(t) \sim (E_0/\rho_0)^{1/5}\, t^{2/5}, \tag{2}$$

where E_0 is the energy released from the target and which generates the shock wave, and ρ_0 is the density of the ambient gas, which is proportional to the gas pressure. In the case of a plane expansion, the propagation law is

$$R(t) \sim (E_0/\rho_0)^{1/3}\, t^{2/3}. \tag{3}$$

Which one of these expansion laws is valid depends again on several deposition parameters, the most important being the laser energy per pulse, the laser spot dimensions on the target, and the deposition pressure.

For all the pressure domains considered up to this point, during the late moments of the plasma expansion the density of the species decreases to the extent that the ablation products can no longer be considered a continuous fluid, so that neither the drag nor the shock model can be applied to model the phenomena. From this moment, the ablation species continue their motion through diffusion.

At pressures over 1 Torr, turbulence appears in the flow of the ablation species [14]. We did not study this domain in detail, since it is over the pressure values used for the deposition of thin films. We will also not go into detail regarding the aspects of the interaction of the species with the substrate, such as reflection of the target species off the substrate [15], since the experimental results we will present here were not made in the presence of a substrate.

Regarding the chemical processes occurring during the PLD plasma expansion, these will depend on the nature of the target species and the ambient gas. In our case, laser irradiation of YBCO targets will produce amounts of Y, Ba and Cu atoms and ions, which can react with the oxygen atmosphere used for depositions, forming oxides. These oxidation reactions will occur either in the gas phase, in the region between the target and the substrate, or on the surface of the substrate, during the deposition itself or during post-deposition annealing in a

gas atmosphere [16,17]. These complex reactions will be discussed in section 4.2, which refers to experimental results obtained using optical emission spectroscopy of the expanding plasma.

3. Fast-framing photography results

3.1 Experimental set-up

The YBCO target was irradiated using a KrF laser delivering pulses of 20 ns duration and energies between 70 and 200 mJ/pulse. The laser beam is focused using an f = 360 mm lens and delivered to the target at a 45° angle (Fig. 1). The energy density on the target can be modified by changing either the energy per pulse or the dimensions of the laser spot on the target; the energy densities used in the present experiments were between 0.3 and 1.5 J/cm^2. The laser energy was monitored continuously during the experiments by reflecting 10% of the beam using a beam sampler and sending it onto a Gen-Tec 500 energymeter coupled to a HP54512B 300 MHz digital oscilloscope.

Fast framing photographs of the expanding plasma were made using a Hadland Imacon model 792 high-speed camera in framing mode. The camera is triggered by a photodiode onto which a small fraction of the incoming beam is incident, either directly or using a variable delay generator; the time reference for the photos is thus the incidence of the laser beam onto the target. A series of either 6 or 8 exposures is obtained for each laser pulse, the interval between two successive photos being 200 ns for 6 photos and 50 ns for 8 photos; the exposure time is 41.2 ns for 6 photos and 10 ns for 8 photos. The delay between the incidence of the laser pulse on the target and the first photograph in the series obtained for one laser pulse is variable between 200 ns (the minimum obtainable delay, due to the internal delay between the trigger and the first exposure) and 5 μs.

Fast-framing photography offers information on the spatial distribution of the species and on their temporal evolution, with very good temporal resolution. However, this information only refers to the excited species which emit at optical wavelengths. In addition, no information regarding the spatial distribution of the emission along the direction of observation can be obtained, so that the spatial evolution can only be seen in one plane at a time (when using one camera, as in our case). The method also does not allow separation of different excited species, since the emission is spectrally integrated. In order to circumvent this limitation of fast-framing photography, optical emission spectroscopy can be used; the results obtained with this method will be described in Section 4.

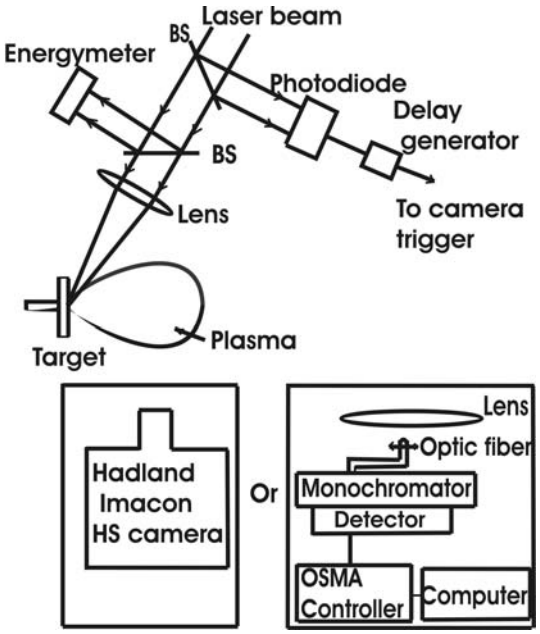

Fig. 1. Experimental set-up for PLD plasma investigation. The analysis was made either using the high-speed camera, or the spectroscopic analysis system. BS are beam splitters.

Experiments were made at pressures between 10^{-5} Torr (considered vacuum) and 20 Torr. In order to separate the hydrodynamic effects from the chemical ones, irradiations were made in oxygen, in which oxidation reactions are known to occur, and nitrogen or argon, for which no chemical reactions should occur or, if any, they would not be of the same nature as for oxygen.

In some cases, a copper ring-shaped electrode was placed at distances between 0.5 and 2 cm in front of the target, parallel to its surface. The ring electrode, having a diameter of 2.5 cm, was centered on the laser spot on the target. dc voltages of different magnitudes and polarities were applied to the electrode; the target was connected to the source ground. The presence of a biased electrode in the plasma improves film quality, presumably through additional activation of species in the plasma [18].

3.2 Experimental results in the absence of a polarized electrode

The deposition pressure is a parameter that strongly influences the behavior of the expanding target species. In vacuum (pressures below about 60 mTorr), the plume has a forward-directed motion along the target normal, without any visible structure (Fig. 2 top). The visible emission has a relatively short duration, ceasing after 1.2÷1.6 μs. In a gas atmosphere at pressures between 60 mTorr and 1 Torr, the behavior of the expanding species in the vicinity of the target is the same as in vacuum, but at larger distances (of the order of several centimeters), a highly luminous front is formed in the presence of a gas (Fig. 2 bottom). The duration of the emission in this case is longer than in the

vacuum case, being over 3 μs, due to this front. Regarding the geometry of the plasma expansion, the motion of the species is less forward-directed than in the vacuum case, due to the collisions of the target species with the ambient gas molecules. (By less forward-directed, we mean that the luminous front propagating in front of the plasma is more curved, and the front has a greater extent in the direction parallel to the target surface.) At pressures over 1 Torr, the luminous front has an irregular shape suggesting turbulence. The pressure limits for the three domains discussed will depend on other experimental conditions; the values given here are valid for our irradiation conditions.

In our conditions, the expansion of the ablated species is independent of the nature of the gas used (oxygen, nitrogen or argon). This behavior seen in fast-framing photos was confirmed by spectroscopic analysis of the plasma. This fact indicates that the visible emission is mostly due to hydrodynamic effects, and not to oxide-forming reactions. Given the similar masses of the nitrogen and oxygen molecules and the argon atoms, it is expected that the hydrodynamic phenomena lead to similar expansion results.

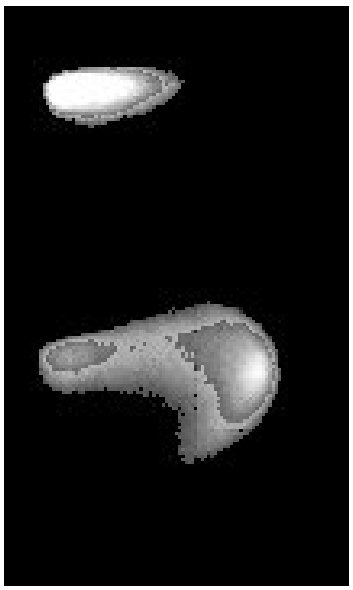

Fig. 2. Fast-framing photographs of the laser ablation plasma. Top: in vacuum; Bottom: in 190 mTorr oxygen. The delay between the incidence of the laser pulse on the target and the photo is 1.2 μs for both photos. The laser energy per pulse is also the same in both cases, 78 mJ.

The energy density on the target is a parameter which affects the geometry of plasma propagation. For a constant energy per pulse of about 100 mJ, if the spot size is increased by defocusing the laser beam from 13 mm^2 (corresponding to about 0.75 J/cm^2) to 23 mm^2 (corresponding to about 0.43 J/cm^2), the motion of the plasma is more forward-directed (Fig. 3).

This effect can be explained in the following way. When the laser spot dimension on the target increases, the emitted target species statistically spend a longer time in the high-density region immediately in front of the target surface before exiting this region through the lateral surface of the plasma, so that the number of collisions per particle increases. According to modeling of the interaction between emitted species, a large number of collisions leads to a more pronounced orientation along the target normal [19,20]. This is due to the properties of collisions, which lead to a "flow" of energy from the velocity component parallel to the target surface to that along the target normal.

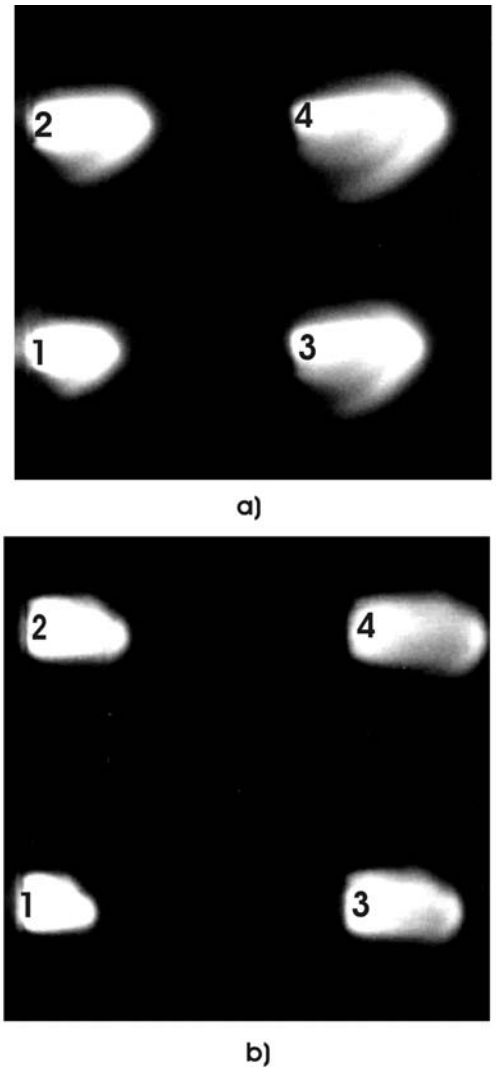

Fig. 3. Plasma expansion for two different laser pulse energy densities on the target: a) 0.75 J/cm^2 (100 mJ; 13.3 mm^2); b) 0.43 J/cm^2 (100 mJ; 23 mm^2). Oxygen atmosphere at 190 mTorr. The photo numbered 1 is taken 600 ns after laser impact on the target. The time interval between two successive photos in a series is 200 ns.

For the largest values of the energy density which we used (1.5 J/cm^2, obtained by increasing the laser energy to 160 mJ) the luminous front has a characteristic "V" shape instead of the rounded one obtained for lower energies.

The plasma structure presents a "tip" which becomes more luminous and propagates with a velocity higher than the rest of the front. This emission could be linked to weak emission which is visible for lower energies, as well, upon scanner examination of the photos (Fig. 4). It probably indicates the presence of the rapid component of the ablation species which we mentioned in Section 2.

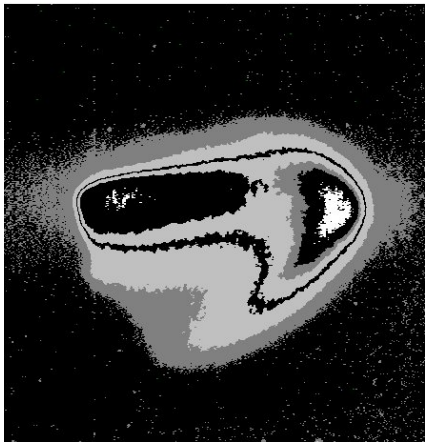

Fig. 4. Image obtained by scanning a photograph obtained in 190 mTorr oxygen, for a delay of 600 ns from the impact of the laser pulse onto the target. Weak emission is visible in front of the luminous plasma front, at its tip. The white regions are the most luminous, followed by the compact black ones around them.

As the pressure increases, the boundary of the front becomes sharp enough to determine its propagation law R(t); R is the distance from the target, measured along the target normal, for the part of the front which moves with the greatest velocity, and t is measured from the incidence of the laser beam on the target. Determination of R(t) allows modeling of the phenomena which occurs during plasma propagation; for moments before the front formation, the following analysis is not possible.

At low pressures, R has a linear t dependence, in accordance with the model for the propagation of the emitted species in vacuum which predicts a constant expansion velocity. The dashed line in Fig. 5, for instance, gives a constant expansion velocity of about 1.6×10^6 cm/s, which is consistent with values obtained by us using another method of plasma analysis, the ion probe [5], as well as with results obtained by other researchers [21,22]. As the pressure is increased, the interaction of the target species with the ambient gas molecules through collisions becomes more important. However, for the first moments, the movement is similar to the motion in vacuum (Fig. 5 and Fig. 6). At later moments (of the order of 600 ns to 1 μs, the exact value depending on pressure and energy density), the motion of the front formed is slowed down, and the motion can be described using the drag (1) or shock model (2, 3). In the case of a spherical shock, $R(t) \sim t^{0.4}$, as given by expression (2); in the case of a plane shock, $R(t) \sim t^{0.67}$, according to relation (3).

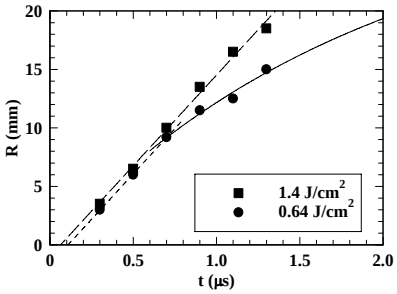

Fig. 5. Expansion of plasma for an oxygen pressure of 60.8 mTorr and two different energy densities. The experimental points are obtained by measuring the distance along the target normal for the part of the front moving with the greatest velocity, at different times from the impact of the laser pulse on the target (for different photos from a set corresponding to the same laser pulse). Dashed line: $R = 15.5t - 0.98$, fit for all points; Full line: $R = R_f[1 - \exp(-\beta t)]$, with $R_f = 29.7$, $\beta = 0.53$, fit for $t \geq 700$ns; Dotted line: $R = 15.5t - 1.68$, fit for $t \leq 700$ ns.

Our experimental data can be fitted well by the above models. In Fig. 5, the curve obtained for 0.64 J/cm^2 has been fitted with a drag model, with parameters $R_f = 29.7$ mm and $\beta = 0.528$ μs^{-1}, which is close to the values of 30 mm and 0.36 μs^{-1} obtained for similar conditions by other authors [7]. Unfortunately, the difference between the curves for the drag and the shock model is significant only at late moments of expansion (over 3 μs), when the luminous front becomes too weak for the R(t) dependence to be determined, so that we cannot say whether the shock or drag model better describe the expansion of the front; for times between 1 and 3 μs, where experimental data exists in our case, the curves are too close to allow us to reach any conclusion (see Fig. 6).

At a given pressure, for large energy densities the propagation of the plasma front is linear for a longer time. In Fig. 5, the plasma moves with a constant velocity over the entire time domain under consideration for 1.4 J/cm^2, while for 0.64 J/cm^2 it is slowed down after about 700 ns. This can be explained by the fact that the target particles are influenced by the ambient atmosphere once the mass of the ambient gas which has been "swept up" by the ablation products becomes comparable with the mass of the ablation products, as we have already mentioned in Section 2. The mass of the ablated products is greater for greater laser pulse energy densities, so that it takes longer for a comparable mass of ambient gas to be swept up.

As illustrated in Fig. 6, the R(t) results obtained from photographs are reproducible. This is proven by the fact that the photographs obtained in the same conditions (same pressure and energy density), but for different pulses are fitted well by the same curves. Again, the linear fit for early times of the expansion is visible ($t < 800$ ns). At later times, both the drag model and the spherical shock ($b = 0.46$, which is close to the $b = 0.4$ expected for the spherical shock, eq. 2) fit the experimental data well. This agrees with recent results obtained for aluminum targets [14]. A curve illustrating the plane shock is also given, which obviously does not fit our experimental data as well.

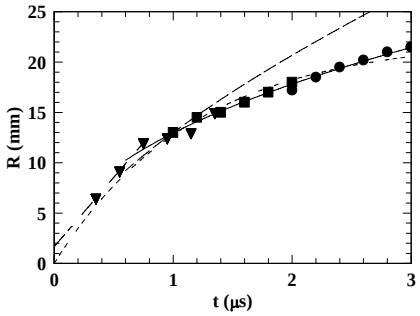

Fig. 6. Expansion of plasma at 190 mTorr, for 1 J/cm^2. The three sets of data points correspond to photographs obtained in the same experimental conditions, for different laser pulses. Fits are as follows: Dash-dot: $R = 13.7t + 1.6$, fit for $t < 800n$; Dot: $R = R_f[1 - \exp(-\beta t)]$, $R_f = 22.3$, $\beta = 0.8$, fit for all t; Full line: $R = 13t^{0.46}$, fit for $t \geq 600$ ns. Dashed line represents plane shock: $R = 13t^{0.67}$.

3.3 Experimental results in the presence of a polarized electrode

The presence of a polarized electrode in the laser ablation plasma leads to more intense visible emission, of an increased duration. The difference compared to the photos obtained without an electrode is especially great in vacuum. We examined the effects of an electrode on the plasma propagation for various distances between the electrode and the target, and for different electrode polarities (positive or negative) and voltage magnitudes.

The effects of the electrode on the plasma evolution are felt for moments subsequent to the time when the plasma reaches the electrode, as seen in Fig. 7. This is observed for all the target-electrode distances investigated (5.7 mm, 8.9 mm, 21 mm). This indicates that the effect of the electrode is through the discharge it initiates in the plasma, as opposed to the effect of the electric field on the plasma species. The hypothesis is also supported by the fact that introducing a large enough resistor in the electrode circuit eliminates any visible effect of the ring on plasma expansion. The discharge current (and therefore the phenomena in the plasma), will depend on how the direction of plasma expansion is related to that of the applied electric field. It is also worth mentioning that it is not the moment when the species excited in the absence of an electrode reach the electrode which is important; rather, it is the moment when the species which only become emissive when a discharge current is initiated in the plasma, and which are not visible in photos in the absence of the electrode, reach it.

The difference between the behavior of the luminous plasma for different polarities applied to the electrode (see Figs. 7, 8) is noticeable both for the early expansion moments (see Fig. 7), and for the late ones (Fig. 8). A difference in behavior is to be expected, given the directionality (and, therefore, the anisotropy) of plasma expansion; however, the exact mechanisms leading to the differences for positive or negative polarity of the electrode could not be given a satisfactory phenomenological explanation at this point in our research.

The intensity of the visible plasma emission is greater for larger voltages, both in duration and in spatial extent. For example, if in the absence of an applied voltage the emission practically dissapears in vacuum after 2 μs, upon applying – 725 V to the electrode it is still noticeable after 4 μs. The probable explanation is that the increased emission is due to the increase of excitation of the existing ablated species. The effect of the presence of the ring electrode is to increase the plasma excitation by collisions between electrons in the discharge initiated through the plasma and the ablated target species. The increased species excitation leads to greater reactivity, which is important for applications.

The effects of the electrode on the PLD plasma will be discussed in more detail in Section 4, referring to optical emission spectroscopy, when more information regarding the nature of the increased plasma emission will be presented.

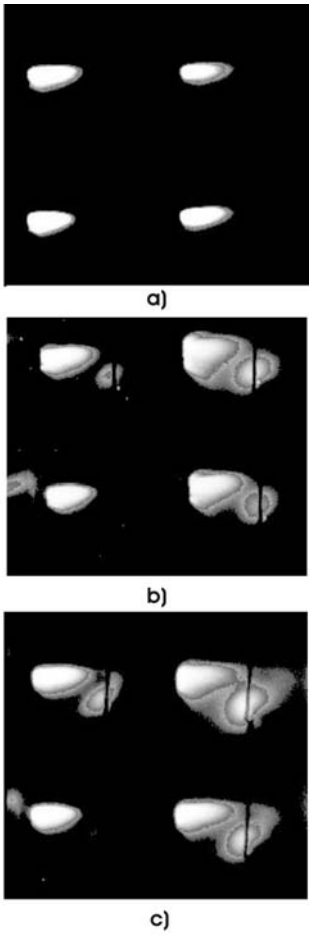

Fig. 7. The effect of the electrode on PLD plasma evolution in vacuum for a 21 mm electrode-target distance. The temporal succession between the images in a series of 4 photographs is: $\begin{matrix} 2 & 4 \\ 1 & 3 \end{matrix}$*. The delay for photo 1 is 600 ns; the time between two successive photos in a series is 200 ns. a) Absence of electrode; b) – 725 V applied to electrode; c) +725 V applied to electrode.*

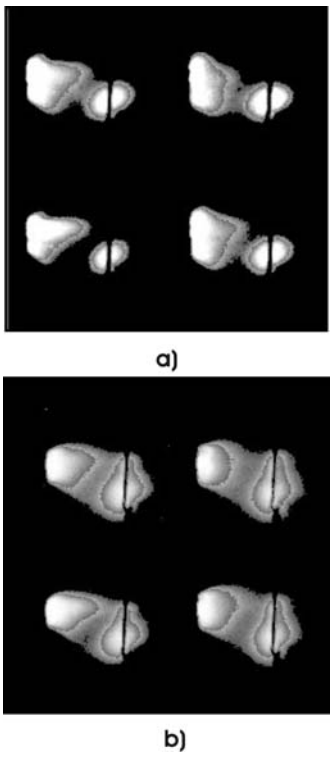

Fig. 8. The effect of the electrode on PLD plasma evolution in vacuum for times > 1μs. 21 mm electrode-target distance. The temporal succession between the images is the same as in fig. 7. The delay for photo 1 is 1.3 μs; the time between two successive photos in a series is 200 ns. a) – 725 V; b) + 725 V.

4. Optical emission spectroscopy results

4.1 Experimental set-up

Spectroscopy was used as a complementary analysis method for fast-framing photography in order to gain insight into the behavior of specific (excited) species. The experimental set-up used is given in Fig. 1. The irradiation geometry is the same as for the fast-framing photos. The spectra were obtained by imaging (with magnification 1) the plasma plume formed in front of the target, using an f = 300 mm lens, onto an optical fiber connected to the entrance slit of a monochromator, which has its 50 μm slit parallel to the target surface. Plasma emission was thus collected parallel to the target surface, for different distances from the target: 0.5 cm, 1 cm and 1.5 cm. The emission was integrated over the total lifetime of the plume. The 320 mm grating monochromator (MC - 25NP Ritsu Oyo Kogaku) has 1200 grooves/mm and a spectral range of 300÷700 nm (compatible with that of the optical fiber). The detector, having 700 channels with 0.055 nm/channel, is connected to a Princeton Instruments OSMA detector controller and a computer for spectrum acquisition. The system was calibrated using a Hg lamp.

The different distances from the target where the spectra were collected were chosen in order to separate the effects due to the target species (in the near-target region) from those due to the presence of a gas atmosphere (front region). The distance of 0.5 cm corresponds to the high-luminosity near-target region which, as discussed in the previous section, is not visibly affected by the presence of the ambient gas. 1.5 cm corresponds to the position of the luminous shock front formed in the presence of a gas atmosphere, as observed in fast-framing photos.

Various pressures were also investigated: vacuum (10^{-5} Torr), 190 mTorr and 500 mTorr, the latter two in oxygen or nitrogen. The effect of a polarized copper electrode described in Section 3.1, placed 2 cm from the target, was studied.

In these conditions, of the lines observed and identified conclusively, the most abundant ones are the atomic and ionic lines of Y and Ba; YII and BaII are predominant (Table 1). Some Cu atom lines are present. No Cu^+ lines are observed, probably due to the relatively high ionization potential of Cu. No lines pertaining to OI, OII or the oxygen molecule or molecular ion were obtained. Of particular interest is the presence of the Y and Ba oxide emission in the 600÷620nm domain. These emissions are important because, as noted above, the presence of oxides is considered essential for good superconducting properties of the deposited YBCO films. No CuO emissions were observed in our experiments; the CuO formation reaction being endothermic, it is energetically unfavorable.

Table 1. The main spectral emission lines identified in our experiments. The intensities given are those observed 1.5 cm from the target, in 500 mTorr oxygen, using energy densities of 1.3÷1.4 J/cm^2. Wavelengths given for the oxides are band heads. Source used for line identification: [23].

Species	λ (nm)	Intensity (arb. units)
YII	371.03	2800
YII	377.43	2900
BaII	389.18	3300
YI	407.74	3000
YI	452.95	2700
BaII	455.40	13 400
YII	488.37	4000
YII	490.01	6500
BaII	493.41	10 000
CuI	510.6	1000
CuI	521.82	1300
YII	520.29	2400
BaI	553.55	2100
BaII	585.37	2500
BaO	564.41	200
YO	597.20	800
YO	600.36	600
YO	601.99	900
BaII	614.17	4700
BaII	649.69	3000

4.2 Experimental results in the absence of a polarized electrode

In this set of experiments the laser energy density on the target was 1.2÷1.4 J/cm^2. In the dense, near target region (0.5 cm from the target), the spectral lines have different characteristics in the small wavelength range (340÷460 nm) and in that of larger wavelengths (> 460 nm). At large wavelengths, the spectra obtained in vacuum, 500 mTorr oxygen and 500 mTorr nitrogen are practically the same for all types of lines (atoms, ions, oxides), as can be seen in Fig. 9. Any small variations can be attributed to variations in laser pulse energy. For instance, the oxide lines have a greater intensity in the oxygen atmosphere compared to vacuum or nitrogen, but this is also the case for the adjacent Ba and Cu lines, which indicates that the difference is generated by pulse-to-pulse variations in laser energy rather than effects of the atmosphere itself.

The similarity in the behavior of the lines is due to the fact that the emissive species are not affected by the presence of gas at this small distance from the target, which agrees with fast-framing photo results.

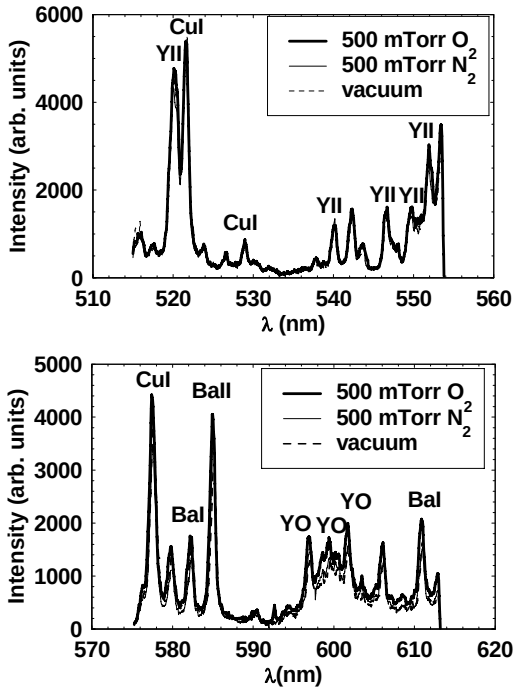

Fig 9. Spectra in two different wavelength domains in the large wavelength range, obtained at 0.5 cm from the target, for different ambient gas conditions.

The fact that the oxide lines (YO) are present in vacuum and nitrogen in the near-target region indicates that (for the laser energy domain used in our experiments) these oxides are emitted from the target.

In the small wavelength region of the spectra of the near-target region, some systematic differences can be observed between the spectral lines obtained in different ambient gas conditions (Fig. 10), the lines in oxygen having lower intensities than those in nitrogen. There is also a relatively intense continuous emission in this wavelength domain, which does not appear at larger wavelengths. The level of this continuous emission is higher in oxygen atmosphere.

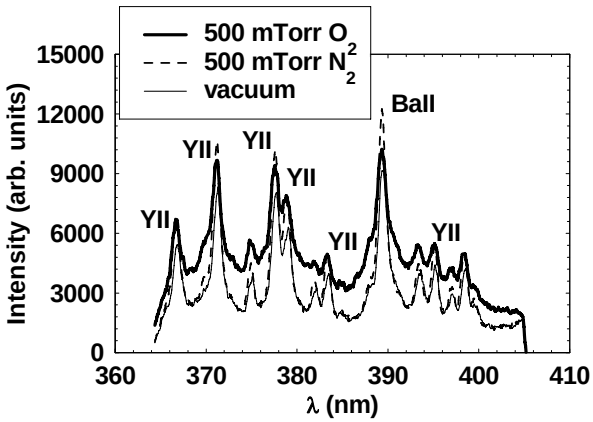

Fig. 10. Spectra in the small wavelength range, obtained at 0.5 cm from the target, for different ambient gas conditions.

The differences in continuous emission can be explained by the presence of numerous O_2 molecule emission/absorbtion bands in the 300÷430 nm range (the Schumann-Runge system, $B^3\Sigma_u^- - X^3\Sigma_g^-$ transitions [23]). These bands generate the continuous emission and its intensity variations (which are associated with emission band variations). The phenomenon which we propose to explain the differences in line behavior is the following. The radiation emitted by spectral lines in this range are absorbed by O_2 molecules (which are present in the O_2 atmosphere) and subsequently re-emitted in a wide band spectrum which appears as a continuum. This results in a decrease of the intensity of target species lines and the increase of the continuous emission in the presence of an O_2 atmosphere. That a continuous emission is present in the case of nitrogen and in vacuum as well is due to the frequent collisions among the target species in the dense near-target region; these collisions lead to ionizations and dissociations, which are followed by radiative recombinations which "feed" the continuous emission. In the case of an oxygen atmosphere, the above-mentioned O_2 molecule band spectrum is superposed over this continuous emission.

Line emission intensity is lower in the luminous region behind the shock front (1.5 cm from the target) than in the near-target region, especially for vacuum expansion (Fig. 11).

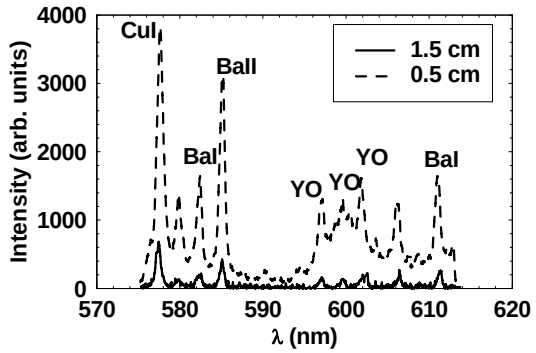

Fig. 11. Variation of spectral line emission with distance from target for YBCO target irradiation in vacuum.

There are more causes for this decrease, the main one being the geometrical effect of plasma expansion which is also visible in the fast-framing photographs. This leads to the decrease of plasma species density. The effect of collisions is also smaller, which means less excited species as well as less continuous emission (and therefore less total emission). However, there is an increase of species density behind the shock front, so that the decrease of emission is less pronounced in the presence of a gas atmosphere than in vacuum (Fig. 12).

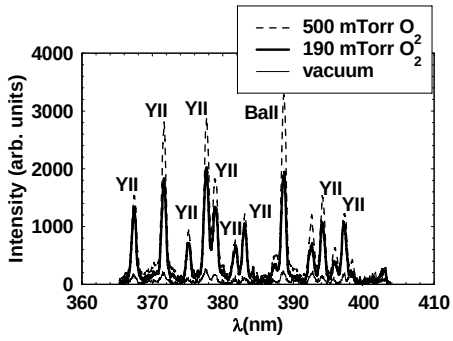

Fig. 12. Dependence of spectral emission on ambient oxygen gas pressure 1.5 cm from target surface.

As expected, at this distance from the target the differences between spectra obtained for different gas pressures is considerable, due to the fact that here the hydrodynamic effects of the gas are felt by the plasma species. Regarding the effect of the gas nature, an oxygen atmosphere leads to stronger oxide line emission in this expansion region than a nitrogen atmosphere, because some of the oxides are produced by gas phase oxidation reactions such as:

$$Y + O_2 \rightarrow YO^* + O,$$

which is an exothermal reaction [24]. However, the differences are not very large when the pulse energies are taken into account by comparing oxide emission to atomic and ion emission (Fig. 13). This means that in the experimental conditions described here, the main mechanism of oxide formation in the plasma is target emission and not gas-phase oxidation reactions. The large luminosity in the front situated about 1.5 cm from the target in a gas atmosphere is thus not mainly due to chemiluminiscent Y-O reactions, but rather to a greater degree of excitation of all species in the high-density region behind the shock front. This emission will not be modified greatly upon changing from an oxygen to a nitrogen atmosphere, since the two gases have similar molecular masses and thermal conductivities.

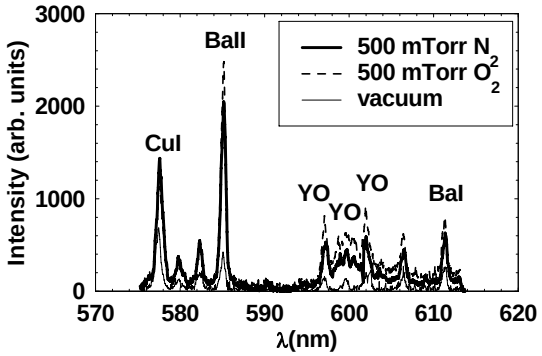

Fig. 13. Dependence of spectral emission on gas nature 1.5 cm from target surface.

It has been suggested that more gas-phase oxidation reactions occur at higher laser energy densities. However, we wish to note at this point that the laser energy densities used in our experiments are in what is considered to be the optimum domain for high-quality YBCO thin films [25-27]. We can thus conclude that the correct oxygen content is incorporated into the film not due to gas-phase reactions, but due to reactions on the surface of the deposited film (either in-situ or after deposition, during the high-temperature phases of film cooling) [28]. This last observation is of obvious practical importance for the deposition of films with good superconducting properties, and it illustrates how important plasma analysis can be for optimizing thin film deposition conditions.

4.3 Experimental results in the presence of a polarized electrode

A study was made of the relative modification of spectral characteristics of neutrals, ions and oxides for different distances from the target, in vacuum and 190 mTorr oxygen, for several magnitudes of positive and negative voltages (240V, 450V). For the experiments described here the energy density was 0.6÷0.7 J/cm^2.

The results show a complicated interplay between parameters. The most interesting result is that, for certain conditions, the oxide emission is greatly enhanced (in comparison to elementary neutrals and ions) in the presence of an applied voltage (both in vacuum and in an oxide atmosphere).

The emitted species observed are the same as those in the absence of the polarized electrode. The relative

intensity from different species depends on various parameters.

Regarding the effect of the magnitude of the applied voltage, the greatest effect is for the increase from 240 V to 450 V (both for positive and negative polarities), the difference between no voltage and +/− 240 V being small.

The dependence on the voltage sign is complex: it depends on distance from the target and voltage magnitude. In vacuum, in the dense near-target region (0.5 cm), the lines obtained for +450 V are up to 3 times more intense than those for −450 V, the difference being more pronounced for the most intense lines (Fig. 14). However, there is an important exception: oxide emission is more intense for −450 V than for +450 V. Oxide emission is also more intense than neutral atom and ion lines in the same spectral range; in fact, for −450 V oxides are more intense than all but a few very strong BaII lines over the entire spectral range studied. For experiments in the absence of an electrode (as already mentioned), in all experimental conditions the oxide emission exhibits low intensity.

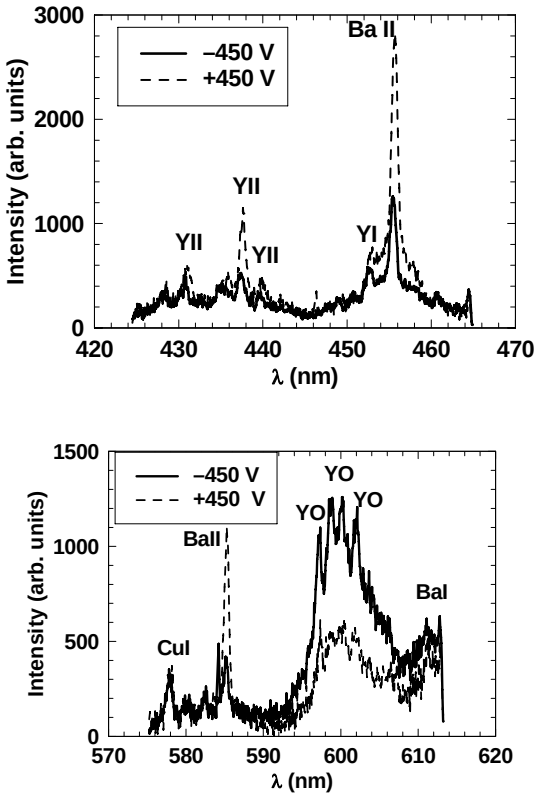

Fig. 14. Spectra observed in the near-target region (0.5 cm from the target), in vacuum, for +450 V and −450 V.

Upon going from 0.5 to 1 cm from the target, there is a decrease in emission intensity which is also observed in vacuum expansion in the absence of an electrode (Fig. 15). A few intense BaII lines are the exception. In the case of −450 V, the decrease in oxide emission is 3 to 4 times greater than for the other species (Fig. 15b). At 1.5 cm from the target, the region close to the electrode, the emission increases (compared to 1 cm) for both positive and negative voltages, as observed in fast-framing photos.

In the regions around 1 and 1.5 cm, the plasma density decreases markedly through expansion in vacuum. A voltage of +450V leads to more intense lines than −450V for all species, including oxides. The phenomenon of intense oxide emission observed in the near-target region is thus no longer present.

In conclusion, in vacuum there is an intense oxide emission characteristic for the high density near-target region, in the case of a negative voltage applied to the electrode. A simple explanation could be proposed. The increase of emission intensity in the presence of an electrode is believed to appear due to greater species excitation produced by electron collisions with plasma constituents [18, 10]. In the case of negative voltages, electrons are strongly accelerated to the dense near-target region, and excite existing oxides (which are normally not visible in emission spectroscopy). This process of excitation followed by radiative deexcitation is for some reason more favorable for oxides than for elementary species in these conditions. In the laser energy density domain used, oxides are emitted from the target; many oxides are not emitted in an excited state, and are only excited by electron collisions. Emission spectroscopy alone cannot completely clarify these processes, a complementary analysis of non-emitting species being necessary.

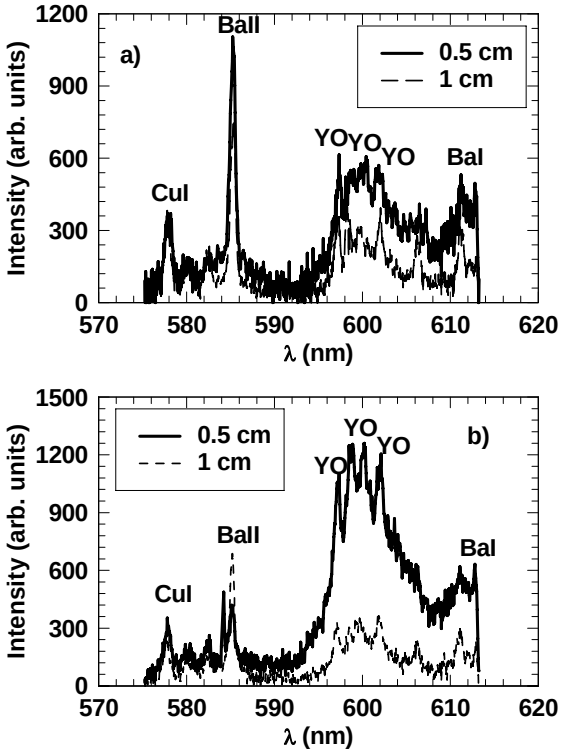

Fig. 15 Variation of spectral line intensity with distance from target for a) +450 V and b) −450 V.

In the presence of a gas atmosphere, some aspects differ from the vacuum case. Experiments carried out in

190 mTorr were only made for +/−240 V, and not higher, in order to avoid a continuous discharge between target and electrode between laser pulses. In our experimental conditions, the luminous front formed behind the shocked gas accounts for most of the emission observed at 1 and 1.5 cm from the target. Both for 1 cm and 1.5 cm, −240 V leads to more intense emission than +240 V for all spectral characteristics, as shown for 1 cm in Fig. 16. This polarity dependence is opposed to that obtained in vacuum, where it was the positive polarity that led to a larger intensity for most species.

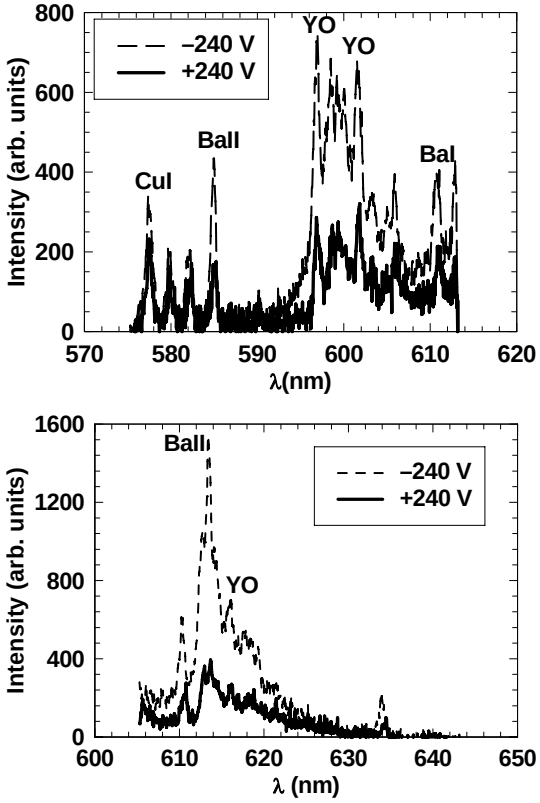

Fig. 16. Spectra observed 1 cm from the target in an oxygen atmosphere of 190 mTorr, for +240 V and −240 V.

Oxide lines are more intense than most lines of the spectrum (exceptions are some intense BaII lines). Spectra at 1.5 cm from the target are similar. It is noteworthy that strong oxide emission appears in the high-density regions of the plasma: the near-target region in vacuum, and the region behind the shock front in a gas atmosphere. The difference between results in an oxygen atmosphere and in vacuum is that in the former case intense oxide emission is for both negative and positive electrode voltages, whereas in the latter only for negative.

There are more possible interpretations for plasma behavior in the presence of an oxygen atmosphere. The first is that in the absence of an electrode, some oxides are formed by gas-phase chemical reactions between Y and O_2, but most of them do not emit radiation. This is either because they are not formed in an excited state, or because they do not emit upon de-excitation. Pramanick and Narayan [29] do in fact state that for molecular species nonradiative relaxation dominates for collisions with gas molecules, while for neutral or ionic atom beams such collisions lead to radiative relaxation. In the presence of a polarized electrode, the spectral emission of these oxides could be preferentially enhanced through electron collisions; the "true" effect of chemical oxide-forming reactions can thus be seen.

The second interpretation is that the presence of a polarized electrode somehow enhances formation of oxides through chemical reactions between ablation products and ambient gas at the contact front. The effect depends on voltage polarity because it is a function of the relationship between the expansion direction of ions and electrons and the direction of the applied electric field [10]. If this second hypothesis is valid, then the increase of YO emission should be associated with a decrease of atomic and ion line emission of Y and O or O_2. We did observe some relative decrease of YII lines (490.01 nm, 520.29 nm), but could not associate this with the variation of OI and OII lines, which are absent in our spectrum. The relative decrease of YI and YII is expected to be small, given the wealth of these lines compared to YO emission.

5. Conclusions

The plasma generated by laser irradiation of a YBCO target was studied using fast-framing photography and optical emission spectroscopy as complementary analysis methods. The deposition pressure has a strong influence on the behavior of the expanding species. However, the nature of the gas used has only a small effect; this is observed both in fast-framing photographs and in spectroscopic data. This implies that hydrodynamic effects are predominant in plasma expansion, while the gas-phase chemical reactions are unimportant. This result is valid for the laser energy densities used in our experiment. Since these energy density values are in the optimum domain for growing YBCO films with good superconducting properties (and therefore with correct oxygen stoichiometries), the proper oxygen stoichiometry for superconducting laser-deposited YBCO thin films is obtained primarily through oxides emitted from the target or created by surface oxidation reactions. This conclusion, which is important for practical thin film deposition applications, is also supported by the fact that oxide spectra is observed not only in an oxygen atmosphere, but in vacuum and nitrogen as well, and by the fact that oxides are observed in the near-target region.

The laser pulse energy density is a parameter which affects the geometry of plasma propagation considerably. For large energy densities, the plasma front structure shows the existence of a “tip” which moves with a velocity greater than the rest of the front, apparently unifluenced by the presence of the ambient gas.

The propagation of the plasma and the effect of irradiation parameters such as pressure and energy density can be modeled well by the shock (2, 3) or drag (1) model, in the presence of a visible plasma front. A

phenomenological model was used to explain these effects.

Complex phenomena were noticed when an electrode with an applied dc voltage is introduced in the laser ablation plasma. The most interesting is that the presence of the electrode can preferentially excite oxides under certain conditions. This enhanced oxide emission is characteristic for the high-density regions of the plasma: the near-target region in vacuum, and the region behind the shock front in a gas atmosphere. This result is potentially important for improving the quality of laser-deposited HTSC thin films. The electrical properties of $YBa_2Cu_3O_{7-x}$ depend strongly on the oxygen content. Therefore, the amounts of oxides which exist in the target-substrate region, as well as their reactivity, can be decisive for obtaining good films.

Most phenomena may be described considering the additional excitation produced by electron collisions in the electrode-target region, after a discharge is initiated in the plasma. The behavior of emissive species alone, however, cannot fully explain why the formation of excited oxides is favored over that of elementary species, or why a positive electrode bias leads to stronger emission than a negative one for 450 V, and weaker emission for 240 V. The clarification of these points, and a more comprehensive description of the process, warrants the use of complementary methods of plasma analysis.

References

[1] C. Ferdeghini, V. Ferrando, G. Grassano, W. Ramadan, E. Bellingeri, V. Braccini, D. Marre, M. Putti, P. Manfrinetti, A. Palenzona, F. Borgatti, R. Felici, C. Aruta, Physica C **378-381**, 56 (2002).

[2] X. F. Wang, O. Li, R.F. Egerton, P. F. Lee, J. Y. Dai, Z. F. Hon, X.G. Gong, Jnl. Appl. Phys. **101**(1), 013514 (2007).

[3] A. H. Li, H. K. Liu, M. Ionescu, X. L. Wang, S. X. Dou, E.W. Collings, M.D. Sumption, M. Bhatia, Z.W. Lin, J.G. Zhu, Jnl. Appl. Phys. **97**(10), 10B107 (2005).

[4] D.H. Youn, J.W. Lee, B.G. Chae, H.T. Kim, S.L. Maeng, K.Y. Kang, Jnl. Appl. Phys. **95**(3), 1407 (2004).

[5] D. Miu, D. Dragulinescu, C. Grigoriu, I. Chis, Optical Engineering **35**(5), 1325 (1996).

[6] The values of the pressure at which one model better describes the phenomena than another actually depend on other irradiation parameters such as the laser pulse energy, since it is actually the relationship between the mass density of the species removed from the target and the density of the ambient gas, as well as the energy of the target species, which determine which model is valid. All of these models, however, treat the ablation products as a continuous fluid.

[7] D.B. Geohegan, Appl. Phys. Lett. **60**(22), 2732 (1992).

[8] D.B. Geohegan in "Pulsed Laser Deposition of Thin Films", Editors: D.B. Chrisey, G.K. Hubler, Wiley, New York (1994).

[9] P.E. Dyer, J. Sidhu, Jnl. Appl. Phys. **64**(9), 4657 (1988).

[10] D. Fried, T. Kushida, G.P. Reck, E.W. Rothe, Jnl. Appl. Phys. **72**(3), 1113 (1992).

[11] D.B. Geohegan, A.A. Puretzky, Appl. Phys. Lett. **67**(2), 197 (1995).

[12] R.F. Wood, K.R. Chen, J.N. Leboeuf, A.A. Puretzky, D.B. Geohegan, Phys. Rev. Lett **79**(8), 1571 (1997).

[13] Y.B. Zel'dovich, Y.P. Raizer, "Physics of Shock Waves and High-Temperature Hydrodynamic Phenomena", Academic Press, New York (1966).

[14] S.S. Harilal, C.V. Bindhu, M.S. Tillack, F. Najmabandi, A.C. Gaeris, Jnl. Appl. Phys. 93(5), 2380 (2003).

[15] A.D. Akhsakhalyan, Y.A. Bityurin, S.V. Gaponov, A,.A. Gudkov, V.I. Luchin, Sov. Phys. Tech. Phys. **27**, 973 (1982).

[16] C.E. Otis, A.Gupta, B. Braren, Appl. Phys. Lett. **62**(1), 102 (1993).

[17] H.F. Sakeek, T. Morrow, W.G. Graham, D.G. Walmsley, Jnl. Appl. Phys. **75**(2), 1138 (1994).

[18] A. Gupta in "Pulsed Laser Deposition of Thin Films", Editors: D.B. Chrisey, G.K. Hubler, Wiley, New York (1994).

[19] I. NoorBatcha, R.R. Lucchese, Y. Zeiri, Jnl. Chem. Phys. **89**(8), 5251 (1988).

[20] J. Haverkamp, R.M. Maya, M.A. Bourham, J. Narayan, C. Jin, G. Duscher, Jnl. Appl. Phys. 93(6), 3627 (2003).

[21] C.E. Otis, P.M. Goodwin, Jnl. Appl. Phys. **73**(4) , 1957 (1993).

[22] F. Claeyssens, S.J. Henley, N.R. Ashfold, Jnl. Appl. Phys. **94**(4), 2203 (2003).

[23] C.R.C. Handbook of Chemistry and Physics, 72-nd Edition, editor D.R. Lide (1991-1992).

[24] H.F. Sakeek. T. Morrow, W.G. Graham, D.G. Walmsley, Appl. Phys. Lett **59**(27), 3631 (1991).

[25] G. Koren, A. Gupta, R.J. Baseman, M.I. Lutwyche, R.B. Laibowitz, Appl. Phys. Lett. **55**(23), 2450 (1989).

[26] B. Dam, J. Rector, M.F. Chang, S. Kars, D.G. de Groot, R. Griessen, Appl. Phys. Lett **65**(12), 1581 (1994).

[27] M.G. Norton, C.B. Carter, Physica C**172**, 47 (1990).

[28] A. Gupta, Jnl. Appl Phys. **73**(11), 7877 (1993).

[29] S. Pramanick, J. Narayan, Jnl. Appl. Phys. **73**(1), 316 (1993).

*Corresponding author: dana.miu@inflpr.ro